Bioconjugate Chemistry

Article

pubs.acs.org/bc

Intracellular Delivery of Luminescent Quantum Dots Mediated by a Virus-Derived Lytic Peptide

Malak Safi,[†,#] Tatiana Domitrovic,[‡,¶] Anshika Kapur, Naiqian Zhan,[†,■] Fadi Aldeek,[†,▽] John E. Johnson,[‡] and Hedi Mattoussi*[,†]

[†]Florida State University, Department of Chemistry and Biochemistry, 95 Chieftan Way, Tallahassee, Florida 32306, United States

[‡]The Scripps Research Institute, Department of Integrative Structural and Computational Biology, MB31, La Jolla, California 92037, United States

Supporting Information

ABSTRACT: We describe a new quantum dot (QD)-conjugate prepared with a lytic peptide, derived from a nonenveloped virus capsid protein, capable of bypassing the endocytotic pathways and delivering large amounts of QDs to living cells. The polypeptide, derived from the *Nudaurelia capensis* Omega virus, was fused onto the C-terminus of maltose binding protein that contained a hexa-HIS tag at its N-terminus, allowing spontaneous self-assembly of controlled numbers of the fusion protein per QD via metal−HIS interactions. We found that the efficacy of uptake by several mammalian cell lines was substantial even for small concentrations (10−100 nM). Upon internalization the QDs were primarily distributed outside the endosomes/lysosomes. Moreover, when cells were incubated with the conjugates at 4 °C, or in the presence of chemical endocytic inhibitors, significant intracellular uptake continued to occur. These findings indicate an entry mechanism that does not involve endocytosis, but rather the perforation of the cell membrane by the lytic peptide on the QD surfaces.

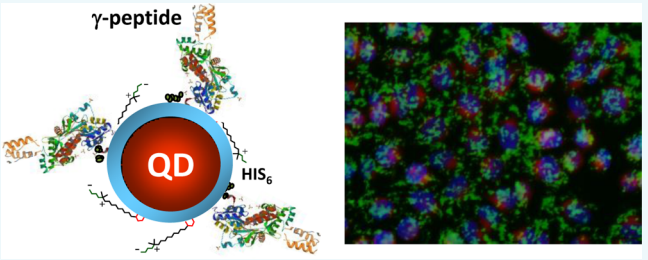

INTRODUCTION

Fluorescence labeling and tracking techniques are required to understand a variety of biological processes, including protein−protein interactions, specific intracellular signaling, and imaging of tissue and cells.[1,2] For decades this approach has relied on the use of organic dyes and fluorescent proteins,[3−5] but more recently fluorescent inorganic nanocrystals have gained interest as they offer additional characteristics that can advance this technology.[6−8] Among those, luminescent quantum dots (QDs) represent a promising platform that has generated much activity in the past decade.[7−12]

These nanocrystals possess several novel size- and composition-dependent photophysical and chemical properties including high quantum yields, broad absorption spectra, narrow symmetric emission profiles, and large achievable Stokes shifts.[7,8,13,14] In addition, due to its large surface to volume ratio, a nanocrystal can be functionalized with multiple biomolecules. These features combined make QDs well-suited for sensing and multicolor in vitro and in vivo imaging.[8,11,15,16]

A few criteria must be met to successfully integrate these materials with biotechnology, including (1) access to high quality hydrophilic QDs, (2) effective schemes to promote their intracellular uptake, and (3) minimal to no cytotoxicity to live cells and tissues. Reports describing QD-bioconjugates that meet all these criteria remain limited.

Two main strategies aimed at promoting the passive delivery of QDs, gold nanoparticles, and magnetic nanocrystals employ either lipid-based transfection reagents,[17,18] or cell-penetrating peptides (CPP).[19,20] These methods typically result in nanocrystals entering the cells via endocytosis, with subsequent entrapment in endosomal/lysosomal compartments.[20,21] Uptake is generally low, even when targeting agents are used with long incubation times. For example, Lee and co-workers recently reported the use of a histidine-rich nona-arginine (HR9) peptide and an INF7 fusion peptide (derived from the influenza virus) also combined with a nona-arginine peptide sequence (IR9), to promote the uptake of QDs by A549 cells.[22] The QD−peptide conjugates were formed via noncovalent interactions with carboxy-rich polymer-encapsulated QDs (e-Biosciences). They reported that QD-IR9 conjugates may enter cells through the endocytotic route, but subsequently escape from the endosomal compartments through the activity of the INF7 fusogenic domain.[23] In another independent study, Galdiero and co-workers tested the ability of a peptide sequence derived from the glycoprotein gH of Herpes simplex type 1 virus, gH625, to promote the intracellular uptake of a few cargo molecules including conjugated-QDs. This peptide interacts with biological membranes, and is believed to contribute to the merging of the viral envelope with the membrane of target cells.[24] The authors reported that the peptide is able to

Special Issue: Interfacing Inorganic Nanoparticles with Biology

Received: October 19, 2016
Revised: December 1, 2016
Published: December 6, 2016

DOI: 10.1021/acs.bioconjchem.6b00609
Bioconjugate Chem. 2017, 28, 64−74

diffuse inside the lipid vesicles and without involving pore formation in the cell membrane, carrying a few distinct cargo molecules. The peptide was conjugated onto the QDs via EDC (1-ethyl-3(3-(dimethylamino)propyl)-carbodiimide, hydrochloride)/NHS (*N*-hydroxysuccinimide) condensation reaction, and when the conjugates were incubated with HeLa cells a sizable internalization was measured. Little to no uptake was measured in the absence of gH625. Electroporation and microinjection were investigated for the introduction of nanocrystals directly into the cytosol,[25−27] and more recently a "mechanical" approach was also described. Here cells were conveyed in a microfluidic device through a constriction channel, where their membranes are transiently disrupted, creating openings that allowed diffusion of QDs into the cytosol.[28] These electrical/mechanical methods are traumatic to the cells and lead to stress and/or damage. Clearly, new effective means to promote the nonendocytotic uptake of nanomaterials by live cells is still needed.

Here, we report a novel method for the benign delivery of QDs conjugated with a 74-amino-acid lytic polypeptide derived from *Nudaurelia capensis* omega virus (NωV), a nonenveloped ssRNA virus that infects insects from the lepidoptera genera (butterflies and moths).[29] A common feature of all nonenveloped animal viruses is a particle-associated lytic peptide that is activated by a chemical cue, which facilitates membrane rupture for genome or particle delivery to the cytoplasm.[30] Although the entry mechanism for most nonenveloped viruses is poorly understood, it is clear that the membrane-interacting polypeptides enable the internalization of particles as large as 90 nm (e.g., rotavirus capsids).[30]

NωV assembles as a pro-capsid and undergoes maturation involving a large conformational change and an autocatalytic cleavage reaction producing the main capsid protein (residues 1−570) and the γ-peptide (residues 571−644).[31] The covalently independent gamma peptides remain associated with the virus particle and disrupt artificial liposomes.[32] The γ-peptides have a hydrophobic N-terminal motif that is predicted to form transmembrane helices (TMpred http://www.ch.embnet.org/software/tmbase/TMBASE_doc.html) and a C-terminal portion containing 8 arginines within the last 17 residues. The high concentration of positively charged residues is a hallmark of cell penetrating peptides, and together with the N-terminal putative TM helix, suggested that this peptide could be an efficient agent for the internalization of nanoparticles.

The polypeptide was genetically fused onto the C-terminal of a maltose binding protein appended with an N-terminal hexa-HIS tag, to facilitate expression of the construct in *E. coli* bacteria. The purified HIS-MBP-γ spontaneously self-assembled onto the QDs through metal−histidine interactions.[33,34] We found that low concentrations (10−100 nM) of QD-MBP-γ assemblies were taken up by three different mammalian cell lines to an extent commensurate with the concentrations and incubation times. Cellular uptake experiments were supplemented by flow cytometry measurements, and results correlated well with the fluorescence microscopy data. Additionally, we combined endosome labeling experiments with incubation in the presence of common endocytosis inhibitors to verify that uptake of the QD-MBP-γ most likely bypasses the commonly encountered endocytotic pathways.

RESULTS

Previous studies showed that the γ-peptide perforates the membrane of synthetic liposomes either when associated with particles as a covalently independent molecule, or as an isolated polypeptide.[32] We reasoned that functionalizing QDs with this γ-peptide would allow the uptake of QD cargos via a non-endocytic pathway. Expression of the γ-peptide in bacteria was inefficient due to induced toxic effects to the host bacteria/cells. However, genetically fusing the gene encoding γ-peptide onto the C-terminus of a hexa-HIS labeled maltose binding protein allowed efficient expression in *E. coli*. In addition, the HIS-MBP-γ construct provided a simple coupling strategy based on metal-affinity coordination between the imidazole groups of the terminal HIS-tag and the Zn-rich QD surfaces (Figure 1A).[33,35−37] Previous studies showed that because such

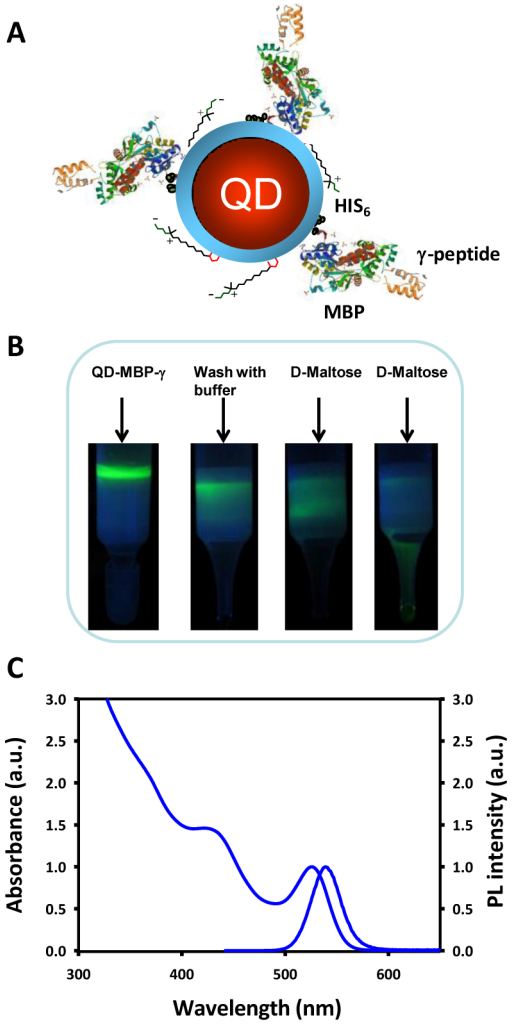

Figure 1. (A) Schematic representation of a QD-lytic peptide assembly; the drawing is not to scale. (B) Binding of the self-assembled QD-MBP-γ conjugates onto amylose column and their release by soluble maltose. (C) Normalized absorption and photoluminescence spectra of the green-emitting QDs used in this study.

interactions require direct coordination between the imidazole groups and the surface of the nanocrystal, this self-assembly provides QD-conjugates with controlled valence and protein orientation.[33,36] For the present system this offers a QD-conjugate configuration where γ-peptide is oriented away from the QD surface for optimal interaction with the cell membrane (Figure 1A).

Self-Assembly of QD-MBP-γ Peptide Conjugates. QDs, prepared following the high temperature injection route,[38] were photoligated with LA-zwitterion ligand producing compact

DOI: 10.1021/acs.bioconjchem.6b00609
Bioconjugate Chem. 2017, 28, 64−74

ZW-QDs that are colloidally stable over a broad range of pH values, and optimally suited for metal−histidine conjugation with proteins.[37] Figure 1C shows the normalized absorption and photoluminescence spectra for green-emitting, ligand exchanged ZW-QDs. The QD-MBP-γ bioconjugates were formed by mixing the $(His)_6$-appended MPB-γ with the ZW-QDs in PBS buffer. The conjugate formation was initially confirmed in vitro using affinity chromatography: binding onto amylose column and release by soluble maltose (Figure 1B). When the conjugate was delivered to a column containing an amylose gel, a fluorescent (green) band attributed to the QD emission was observed under UV excitation, confirming the presence of MBP on the QDs. The band was stable after several washes with PBS buffer, but was readily eluted after addition of 2−3 mL of 20 mM solution of D-maltose; the latter binds with greater affinity to MBP than amylose. These data clearly showed that the self-assembly between ZW-QDs and His_6-MBP-γ took place and that the MBP maintained its specific activity. In addition, access to the maltose-binding pocket requires significant exposure of the protein, demonstrating that MBP, and consequently γ-peptide were exposed on the QD surface, consistent with the conjugate configuration shown in Figure 1A. The preserved biological activity of MBP after immobilization on the QDs is in full agreement with previous findings, where conjugate formation was further characterized by gel electrophoresis and dynamic light scattering (DLS) measurements. The latter show that there is an increase in the overall hydrodynamic radius of the QD−protein conjugates (compared to the unconjugated QDs) that is commensurate with the number of MPB attached per QD.[27,39]

Intracellular Uptake. We explored the effects of QD concentration, incubation time, temperature of incubation, and endocytic inhibition on the degree of intracellular uptake, applied to three sets of eukaryotic cells, HeLa, HEK293, and NIH/3T3. The cells were prepared and tested with three sets of QD dispersions: unconjugated QDs, QD-MBP conjugates, and QD-MBP-γ conjugates; the QD-conjugates were self-assembled with MBP or MBP-γ at a molar ratio of 1:10. Incubation with QDs and QD-MBP was used as control experiments.

First, HeLa cells were incubated either with varying concentrations of QD-MBP-γ for a fixed incubation time or with a fixed concentration of reagents while varying the time of incubation. Each row of panels in Figures 2 and 3 shows representative differential interference contrast (DIC) and fluorescence images corresponding to the distribution of DAPI nuclear staining (blue), QDs (green), Cy5-transferrin (Cy5-Tf, red), and the merged images. Figure 2B shows that when cells were incubated with the conjugates for 30 min the characteristic fluorescence of the QDs (green) increased commensurately with increasing QD-conjugate concentrations.

Figure 3A,B shows that with incubation times of 10 min and 1 h at 10 nM or 100 nM of the conjugates, the internalization of QDs was proportional to the incubation time. Incubation of cells with the control solutions of QDs only or QD-MBP conjugates (no γ-peptide) produced negligible intracellular green emission for the same concentrations and incubation time (Figure 2A). Additional data on the peptide mediated uptake of QD-MBP-γ bioconjugates by NIH/3T3 and HEK293 cells are provided in the Supporting Information, Figures S2 and S3.

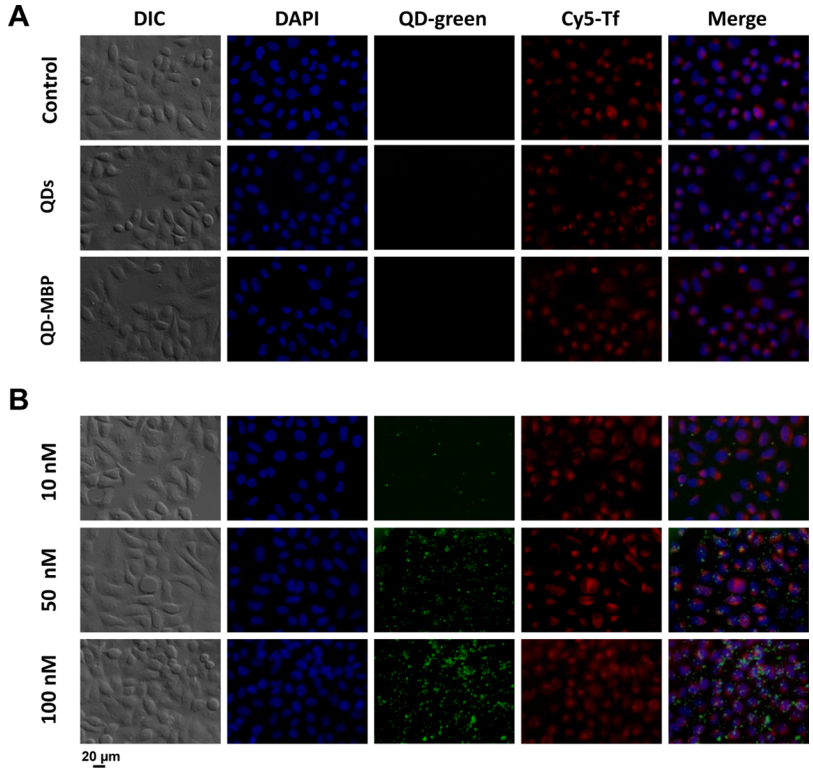

Figure 2. Effect of QD-conjugate concentration on the intracellular uptake. Images collected from HeLa cells incubated with nonconjugated and conjugated QDs at 37 °C for a fixed incubation time of 30 min. (A) Cells incubated with 50 nM of QDs and QD-MBP along with control culture. (B) Cellular uptake of QD-MBP-γ bioconjugates incubated at different concentrations. The DIC and epi-fluorescence images were collected using a 40× magnification objective.

DOI: 10.1021/acs.bioconjchem.6b00609
Bioconjugate Chem. 2017, 28, 64−74

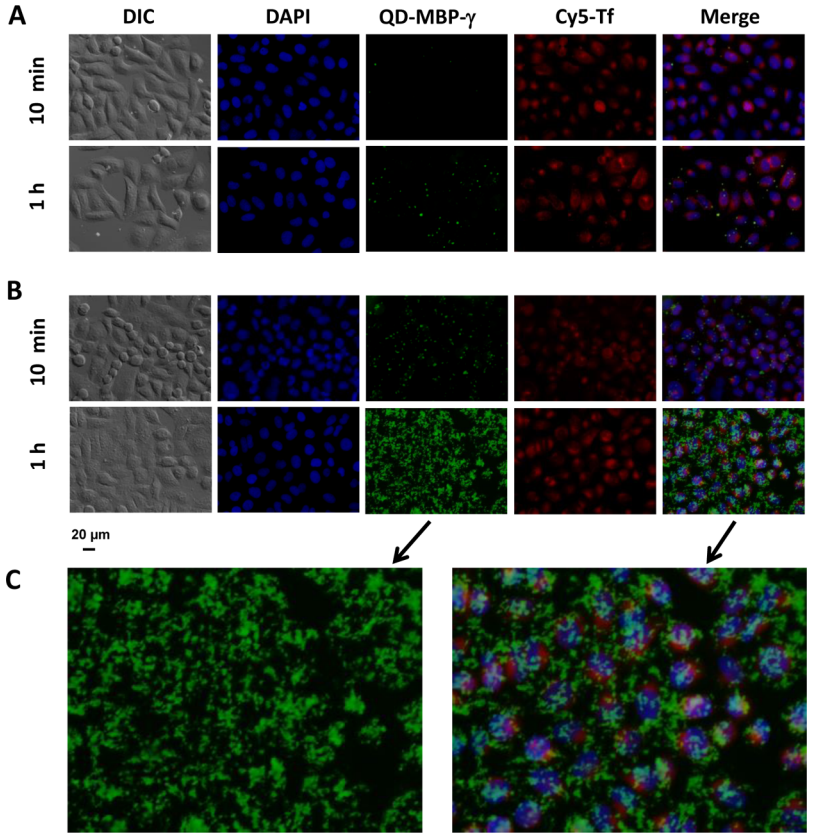

Figure 3. Effect of the incubation time on the intracellular uptake for a fixed concentration of QD-MBP-γ conjugates. Images collected from HeLa cells incubated with conjugates at 10 nM (A) and at 100 nM (B). Incubation was carried out at 37 °C and images (DIC and epi-fluorescence) were collected using a 40× objective. (C) Expansion (by 250%) of the indicated panels shown in B.

Intracellular Distribution of QD-MBP-γ Does Not Correlate with Endosomes. Confocal microcopy imaging was used to track QD-conjugates inside cells coincubated with Cy5-transferrin (red), a recycling endosome marker.[40,41] Indeed, the fluorescence signals were found in significantly different regions of the cells; the Cy5 emission was largely found in the perinuclear region, while that of the QDs was distributed throughout the cytoplasm but not in the nucleus (see Figure 4B). Confocal fluorescence images collected at different focal planes along the vertical axis showed that the QD signal was limited to the intracellular volume with the maximum distribution localized in the middle of the cell (where the DAPI signal was also the highest). QD fluorescence decreased to background levels when the focal plane was moved away from the middle of the cell (see Supporting Information Figure S4). These data combined prove that inside the cells the QDs are not associated with endosomes, and suggest an uptake mechanism that does not involve endocytosis.

To complement and support the above findings, namely, that QD-MPB-γ conjugate transfer through the plasma membrane is likely the driving mechanism, we carried out two sets of experiments: (1) Cellular uptake was studied at lower temperature (4 °C); and (2) incubation in the presence of sodium azide and sucrose. Incubation at lower temperature (4 °C) has been used as one of the means to block endocytosis, while NaN_3 and sucrose are reported chemical inhibitors of endocytosis, via ATP depletion and blocking of clathrin-mediated endocytosis, respectively.[9,20,42−47] Data show that although the process of endocytosis is reduced in cells incubated with the conjugates at 4 °C, sizable amounts of intracellular uptake of QD-MPB-γ conjugates persisted as indicated by the measured green emission (see Figure 4B, panel g). Similar results were collected when the cell cultures were pretreated with solutions of 10 mM NaN_3 and 50 mM 2-deoxy-D-glucose for 30 min, or preincubated with 0.4 M sucrose solution for 1 h, prior to incubation with the QD-MBP-γ conjugates. The images shown in Figure 4, panels h and i, show that here too cells can readily internalize QD-conjugates under these conditions. Nonetheless, uptake is slightly reduced under these inhibitory conditions in comparison to normal conditions. In comparison, no measurable Cy5-transferrin staining was observed at 4 °C, indicating that virtually no endocytosis occurred under these conditions. Furthermore, no uptake was detected for nonconjugated QDs at 4 °C (Figure 4B, panel j). These findings combined with the confocal images shown above strongly suggest that internalization of the QD-MBP-γ primarily occurs via translocation through the membrane; some levels of endocytosis-driven uptake may still be present, nonetheless.

These findings contrast with experiments carried out by our group using similarly capped QDs, coupled to cell penetrating peptides, either via metal−histidine conjugation (e.g., using the sequence His_8-Trp-Leu-Ala-Aib-Ser-Gly-$(Arg)_8$-amide), or via covalent coupling, where QD intracellular staining was consistently found to coincide with the endosomal distribution.[20,48] The latter were visualized using a red-emitting dye-attached to a transferrin protein, as done in this study.

Flow Cytometry Measurements. Flow cytometry complements the imaging data by providing the average fluorescence of the cellular ensemble when incubated with the above QD-MBP-γ conjugates. The intracellular fluorescence,

DOI: 10.1021/acs.bioconjchem.6b00609
Bioconjugate Chem. 2017, 28, 64−74

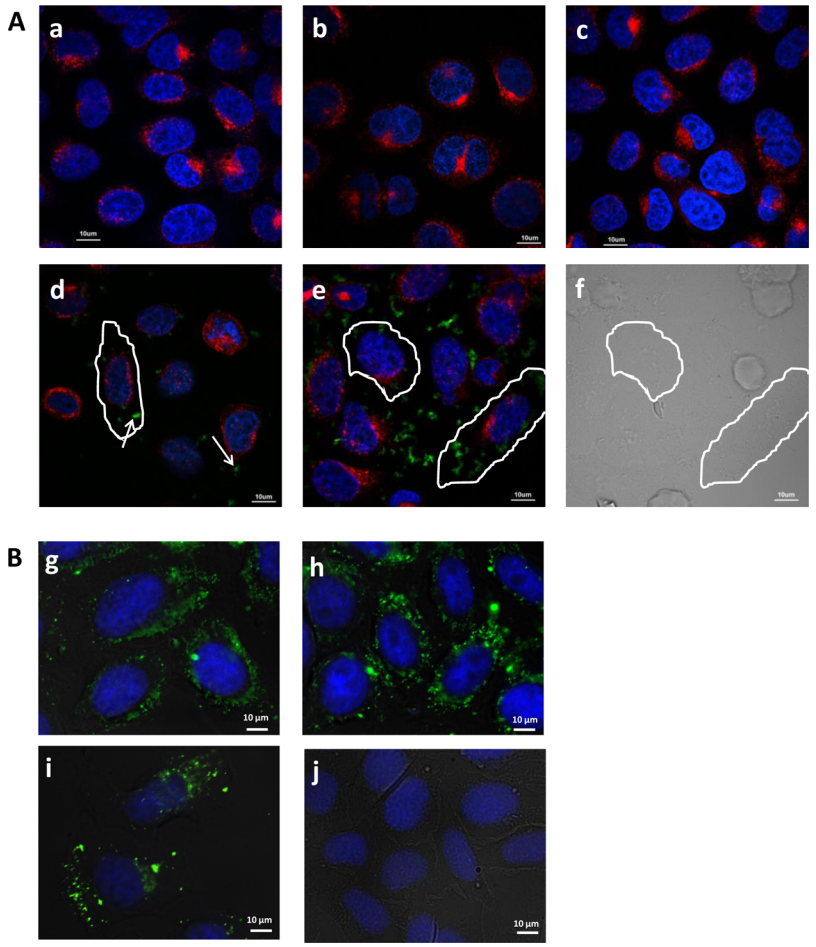

Figure 4. (top panels, A) Confocal microscopy images of HeLa cells incubated with QD-bioconjugates for 30 min at 37 °C. Shown side-by-side are control culture without QDs (a), and cells incubated with 50 nM unconjugated QDs (b), 50 nM QD-MBP (c), 50 nM QD-MBP-γ (d), and 100 nM QD-MBP-γ (e); the DIC image (f) corresponds to the fluorescence image shown in panel (e). Arrows indicate the QD internalization (green). Endosomal compartments and nuclei are stained with Cy5-apo-transferrin (red) and DAPI (blue), respectively. Images collected using a 60× objective. (bottom panels, B) Images collected from HeLa cells incubated for 40 min with 100 nM QD-MBP-γ conjugates, at 4 °C (g), in the presence of 10 mM NaN_3 (h) in the presence of added sucrose (i), and with QDs at 4 °C, control (j).

associated with the QDs, was quantitatively determined by measuring the fluorescence intensity with a 525/50 nm filter and a laser excitation at 405 nm.[49] Cells incubated with QD-MBP-γ at 50 nM for 10 min, had a fluorescence intensity corresponding to a labeling efficiency of ∼18% (i.e., 17.7% of the cell population was labeled with QD-MBP-γ, Figure 5C). At the same concentration, incubation times of 30 min and 1 h, produced fluorescence intensity corresponding to 80.4% and 95% of the cells being labeled (Figure 5D,E). A negligible signal was measured for cells incubated with QDs only (Figure 5B). A quantitative bar graph describing these measurements is shown in the Supporting Information (Figure S5).

Cells Permeated with QD-MBP-γ Remain Fully Viable for Multiple Generations. The MTT (3-(4,5-dimethylthiazol-2-yl)-2,5-diphenyltetrazolium bromide) cell viability assay was employed to determine the cytotoxicity of QD-MBP-γ. Reduction of MTT to formazan by mitochondrial enzymes produces an absorbance at 570 nm that can provide a direct measure of mitochondrial activity and cell vitality. HeLa cells were incubated with QD-MBP-γ conjugates at concentrations between 6.25 nM and 100 nM for 90 min, followed by rinsing and further culturing for 24 h. Absorption measurements were then performed with a TECAN spectrophotometer (Infinite M1000). The data summarized in Figure 6C show that cell viability remained at ∼100% and comparable to the viability measured for cells incubated with unconjugated QDs or QD-MBP conjugates. Thus, cells permeated with QD-MBP-γ display normal mitochondrial activity, in good agreement with previous findings, and indicate that these colloidally stable QD conjugates elicit no toxic effects at nanomolar to micromolar concentrations.[20,50,51]

Following Extended Incubation Intracellular QD-MBP-γ Diffuses and Partially Localizes to Lysozomes. HeLa cells were tested under conditions of acute exposure to the QD-MBP-γ, and cultures were monitored over longer periods of time to determine the fate of the conjugates. Cell cultures were first incubated with the QD-MBP-γ at high concentration (100 nM) for 90 min followed by rinsing and subsequent culture for 6, 12, and 24 h. Figure 6A shows that following incubation, the QD-associated green fluorescence was pronounced and distributed in regions of the cells that are distinct from those of recycling endosomes. Subsequently cultured cells continued to proliferate at a rate similar to those measured for control cultures, with no change in density or morphology. Following periods of cell division the green signal weakened and dispersed in the cytosol, but gradually localized closer to the nucleus (Figure 6A, panels b and c). In particular, after 24 h

DOI: 10.1021/acs.bioconjchem.6b00609
Bioconjugate Chem. 2017, 28, 64−74

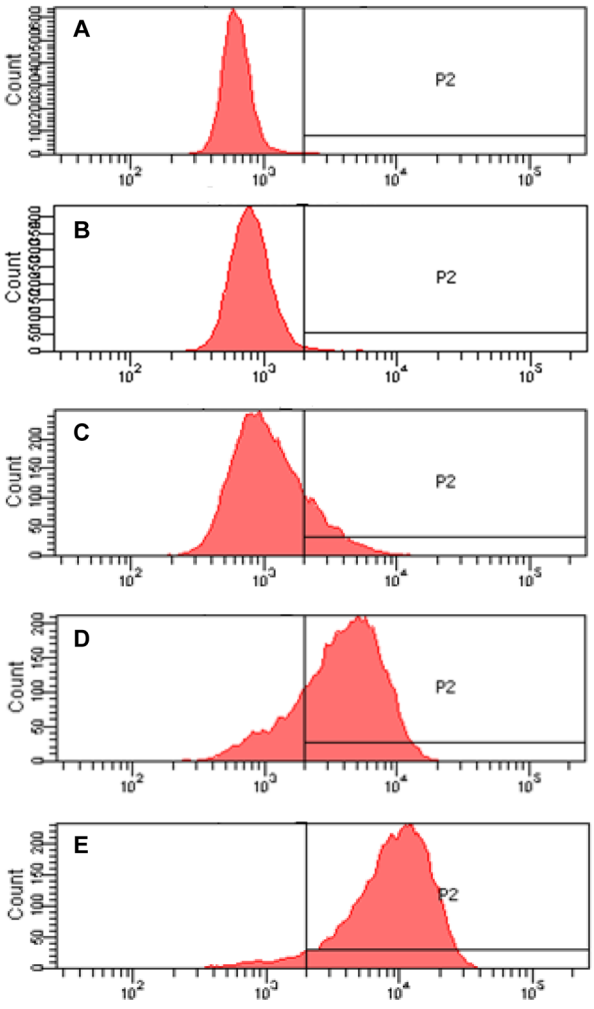

Figure 5. Quantitative assessment of QD uptake by HeLa cells using flow cytometry. Cells alone (A); cells incubated with 50 nM QDs (B); cells incubated with 50 nM QD-MBP-γ at 37 °C using incubation times of 10 min (C), 30 min (D), and 1 h (E). P2 designates the percent fluorescence labeling of the cells; P2 = 0.2% (A, control), P2 = 1.1% (B), P2 = 17.7% (C, 10 min), P2 = 80.4% (D, 30 min), and P2 = 95% (E, 1 h).

of culturing, we observed moderate colocalization of QD fluorescence with Cy5-transferrin, indicating that some of the conjugates reside in multivesicular body-like structures (Figure 6A, panel d) long after entry. DIC images in Figure 6B show that cell morphology and density were essentially identical for cultures incubated with QDs, QD-MBP-γ conjugates and control cultures not exposed to any reagents.

DISCUSSION

The above results indicate that QDs self-assembled with MBP-lytic-peptide interact with live cells in a drastically different manner compared to cells incubated with pure QDs or QDs conjugated to cell-targeting biomolecules, including cell penetrating peptides, RGD peptides, and receptor-targeting molecules (e.g., folic acid,[52] epidermal growth factor (EGF),[53] transferrin,[54] extracellular enzymes such as matrix metalloprotease 2 [MMP-2] and MMP-7,[55] and cholera toxin subunit B (CTB)).[56] All the latter delivery vehicles resulted in QD-conjugates sequestered within endosomal compartments, and essentially isolated from the cellular machinery. In contrast, the γ-peptide promotes a highly efficient pathway for the

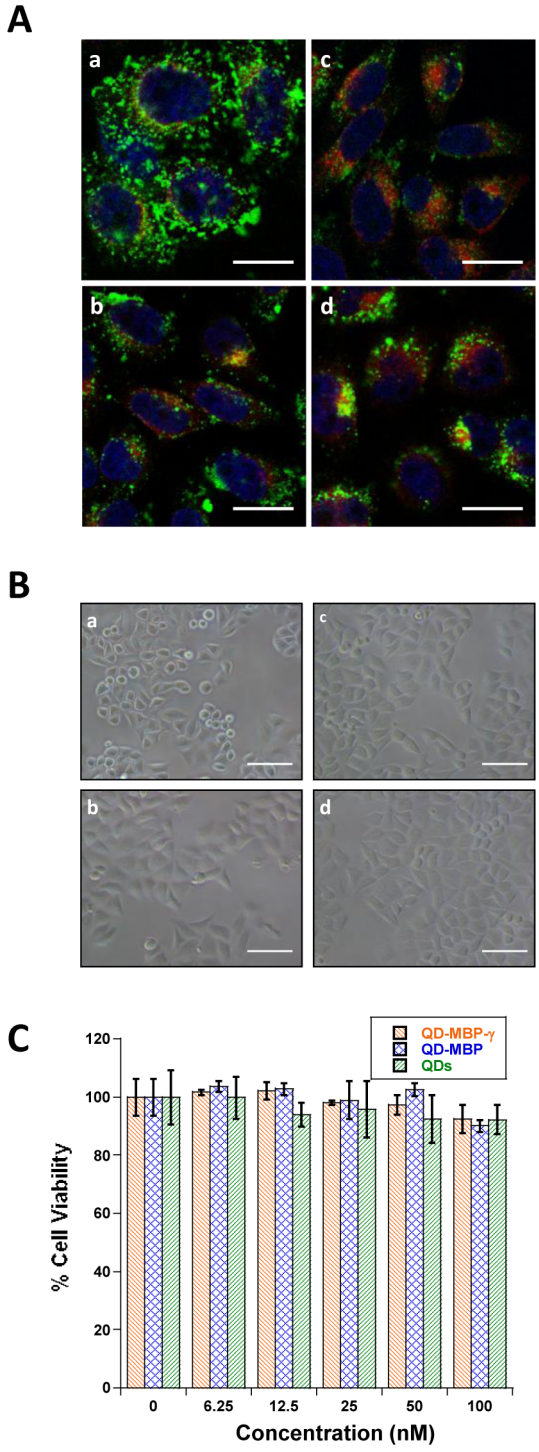

Figure 6. (A) Fate of the QD-MBP-γ inside cells following uptake and culturing. Representative confocal microscopy images (magnification 60×) of HeLa cells incubated for 90 min at 37 °C with 100 nM QD-MBP-γ. The cells were then washed twice with PBS 1× and incubated with fresh media for (a) 1 h 30 min, (b) 6 h, (c) 12 h, and (d) 24 h; scale bar = 30 μm. (B) DIC images of the above cell cultures shown side-by-side with control culture. After 90 min of incubation with the conjugates, the cells were washed and cultured in fresh media for 24 h prior to imaging. Images shown are from cells incubated without QDs (a, control), QDs (b), QD-MBP (c), and QD-MBP-γ (d). Scale bar = 100 μm. (C) MTT viability assay conducted on HeLa cells incubated with 100 nM of the QD reagents for 90 min, washed with PBS buffer, and cultured in fresh media for 24 h prior to data collection.

DOI: 10.1021/acs.bioconjchem.6b00609
Bioconjugate Chem. 2017, 28, 64−74

intracellular uptake of QD cargos that does not involve endocytosis. This conclusion is confirmed by the high levels of intracellular uptake of QD-MBP-γ even for relatively short incubation times. It is further supported by fluorescence data collected from cells incubated with QD-conjugates at 4 °C and in the presence of commonly used endocytosis inhibitors, where a sizable uptake of QD-MBP-γ is measured for HeLa cells (Figures 3 and 4). In addition, comparable intracellular entry and distributions of QD fluorescence is observed across multiple types of cell lines. These results demonstrate a major role played by the lytic peptide in facilitating nonendocytotic uptake of the QD-conjugates.

In its normal setting, the γ-peptide is generated as part of the virus maturation program by an autocatalytic cleavage of the capsid protein where residues 571−644 are covalently released from the sequence 1−570. The crystallographic structure of NωV virion shows that the γ-peptides are not exposed to the external environment and remain noncovalently associated with the virus.[57] Therefore, the virus lytic activity depends on the dynamic motions of the capsid that allow γ-peptide exposure and interaction with cellular membranes. This exposure is regulated by pH and, contrary to viruses that are activated by the acidic pH in the late endocytotic vesicles, NωV is only active above pH 7.[32] This mechanism relies on the electrostatic interactions that dominate the contacts between the capsid subunits. At pH 5.0, repulsion forces generated by negatively charged amino acid residues on the subunit interfaces are neutralized by protons and the capsid is stable and compact.[58] The γ-peptides are immobilized inside the capsid under these conditions and no lytic activity is detected. Increasing the pH removes protons and negatively charges the juxtaposed acidic residues between the subunits resulting in exposure of the gamma peptides. This unusual regulation has led to the hypothesis that NωV uses the alkaline environment of the Lepidoptera midgut as an activation cue for infection, and virus entry occurs through the plasma membrane, independent of the endocytotic pathway.[32] Although the timing of the exposure is controlled by the capsid, studies of the isolated γ-peptide (released after heating mature virions followed by purification and pelleting of the particles) have shown that its lytic activity profile is also highest above pH 7.

The biological properties of γ-peptide made it an obvious candidate for use as an entry vehicle that could directly breach the plasma membrane. However, all efforts to express it alone, or as a HIS-tagged polypeptide, resulted in bacterial toxicity and vanishingly small yields of γ-peptide product. However, expression was dramatically enhanced when the gene for γ-peptide was fused to the C-terminus of a N-terminal HIS-tagged MBP gene, creating a HIS-MBP-γ (~50 kDa). This construct spontaneously self-assembled onto ZW-QDs through the HIS tag and permitted easy purification of the QD-conjugates via affinity chromatography using amylose gel. QD-HIS-MBP-γ cell entry was exceptionally efficient, with internalization even at 4 °C and in the presence of NaN_3 and sucrose, suggesting an entry route that primarily is independent of the endocytotic pathways.

The ability of the cells carrying rather large loads of these assemblies to proliferate at levels comparable to those of control cultures several hours post uptake, while dividing the amount of QD-conjugates among daughter cells, reflects the absence of any toxic effects of the QD-conjugates. This is a clear benefit of the stability of the inorganic core of the QDs afforded by the strong and inert capping ligands used. It also reflects the inert nature of the MBP-γ fusion to the intracellular machinery. The progression of the intracellular distribution of the QD signal several hours following uptake, namely, the partial colocalization with the Cy5-transferrin signal, may be attributed to a process of autophagocytosis (or autophagy), which is known to involve the capacity of live cells to treat and degrade materials that are either unnecessary, or do not possess defined biological functions/activities. In such processes, live cells degrade damaged or obsolete organelles and proteins in the cytoplasm, starting by the formation of membrane "sacs" called phagophores that engulf a portion of the cytoplasm leading to the formation of the phagosomes. These will fuse to lysosomes forming autophago-lysosomes responsible for removing undesirable proteins and defective organelles. The process of autophagocytosis has been observed in HeLa cells and has been described in studies of other types of nanoparticles.[59−61]

We would like to note that following uptake, the QD signal distribution is not fully homogeneous. The in vitro stability tests of our QDs in the cellular media eliminate the argument of their aggregation inside cells. The punctate signal may be attributed to a few possibilities: (1) The combined charge of a fraction of QD−peptide conjugates resulting from the positively charged peptide and the effectively negatively charged zwitterion coating may lead to electrostatic interactions with the intracellular organelles; (2) The lytic property of the peptide might also direct the conjugates to intracellular organelle membranes observed as punctate. Further, we do observe that with longer incubation periods the nanoparticle shows vesicular entrapment that is expected for unnecessary foreign materials inside cellular environment. Future experiments focused on investigating the intracellular targeting of the peptide and QD-conjugates will provide additional insights into the fate of the assemblies inside cells.

CONCLUSION

We have detailed the use of a 7.7 kDa lytic peptide derived from the *Nudaurelia capensis* Omega virus to promote the intracellular uptake of luminescent QDs via a mechanism that circumvents endocytotic pathways. The γ-peptide was fused onto a polyhistidine-terminated maltose binding protein to allow efficient expression in *E. coli* bacteria. The HIS-MBP-γ was then self-assembled onto ZnS-overcoated QDs via a simple procedure that provides control over the protein orientation in the conjugate. The intracellular uptake of the QD-MBP-γ assemblies was shown to be efficient and dependent on the QD concentration, incubation time, and temperature. Furthermore, the intracellular distribution of these peptide-modified QDs was found to be distinguishable from that of recycling endosomes. The biodistribution of the QD-MBP-γ indicated that during cell division the bioconjugates were passed from mother to daughter cells and migrated to the perinuclear region, with no obvious physiological changes of the cells. Cells containing these assemblies proliferated at rates comparable to those of control cultures several hours post uptake. This combined with the near 100% viability of the cells (tested with the MTT assay) indicate that these assemblies do not elicit any measurable cytotoxic effects to live cells.

This is a promising finding as this HIS-MBP-γ can be applied to promote the uptake of a variety of other nanoparticles. For example, we showed recently that protein self-assembly onto Au nanoparticles promoted by metal-HIS coordination is highly efficient.[62] The intracellular entry described here can also

DOI: 10.1021/acs.bioconjchem.6b00609
Bioconjugate Chem. 2017, 28, 64−74

advance the integration of these inorganic platforms into biotechnology and allow better exploitation of their unique properties. Additional studies of the peptide may identify shorter sequences of γ that retain the described entry functions, making it feasible to produce it by chemical synthesis.

EXPERIMENTAL SECTION

Peptide Cloning Expression and Purification. The gamma peptide DNA sequence (residues 571−644) was amplified and cloned into the plasmid pMAL-C2X (New England Biolabs) using the restriction enzymes Xmn1 and *Bam*HI. The recombinant plasmid was digested with NdeI and *Bam*HI enzymes, releasing a fragment starting at the first ATG of the maltose binding protein (MBP) gene and containing the gamma peptide gene fused onto the 3′ end of the MBP gene creating a MBP-γ at the protein level. The fragment was cloned into the plasmid pET28a (Novagen), which contains the gene for a N-terminal hexahistine tag. The sequence integrity and correct insertion were confirmed by sequencing.

E. coli Bl21-DE3-Rosetta bacteria (Novagen) were used for protein expression. Briefly, freshly transformed bacteria cells were inoculated into Luria−Bertani broth supplemented with 0.2% glucose and grown at 37 °C. The temperature was adjusted to 28 °C, and expression was induced by adding 1 mM IPTG and further carried out for 4 h. Cells were collected by centrifugation, suspended in lysis buffer [50 mM Tris pH 7.6, 150 mM NaCl, EDTA-free protease inhibitors (Roche), 0.5× Bug Buster reagent (Novagen)] and sonicated on ice to avoid sample heating. Cell debris were pelleted by centrifugation (12 000 g at 4 °C) and the supernatant subjected to the first purification step using immobilized metal (Ni^{2+}) ion affinity chromatography (His-trap-GE-Healthcare Life Sciences). After elution using an imidazole gradient, the fraction enriched with the recombinant protein was further purified using amylose resin (New England Biolabs). The recombinant protein was then eluted with 10 mM maltose. The maltose was removed and the protein was concentrated in PBS using 10 kDa centrifugal filter (Amicon-Millipore), and the protein purity and quality was confirmed by mass spectroscopy (MALDI-TOF analysis).

Quantum Dot Growth and Phase Transfer. We used CdSe-ZnS core−shell QDs with emission centered at 545 nm, corresponding to a core−shell diameter of ∼6 nm.[13,63] They were synthesized in two steps (growth of the core followed by ZnS-overcoating) using high temperature reduction of organometallic precursors in coordinating solvent mixtures made of alkylphosphines, alkyphosphine-carboxyl, and alkylamines, as described in previous reports.[38,64,65] The native hydrophobic TOP/TOPO capping ligands were further exchanged with zwitterion-appended lipoic acid (LA-zwitterion) ligand using a photoligation strategy to render the nanocrystals hydrophilic and biocompatible.[66] This approach relies on the photochemical reduction of the dithiolane groups, combined with competitive displacement of the native ligands and coordination of the zwitterion ligand onto the nanocrystals. Importantly, capping the QDs with zwitterion ligand, instead of PEGylated ones, permitted the easy implementation of the QD self-assembly with polyhistidine-appended proteins (MBP-His and mCherry-His), driven by metal-histidine coordination as detailed in previous studies.[37]

Assembly of Quantum Dot−MBP-γ-Peptide Conjugates. The QD-MBP-γ conjugates were formed using a molar ratio of MBP-γ:QD of ∼10:1. We briefly describe the procedure for preparing a solution of QD-MBP-γ conjugate at a concentration of 100 nM. 6.6 μL of $(His)_6$-MBP-γ stock solution (conc. ≅ 75 μM) was added to 17.4 μL PBS buffer (pH 7.9, 10 mM) in an Eppendorf tube. In a separate Eppendorf tube, 6 μL of a stock solution of ZW-QDs (conc. = 8.3 μM) was diluted with PBS buffer (pH 7.9, 10 mM) to a total volume of 26 μL. The solution of $(His)_6$-MBP-γ was then added to the tube containing the dispersion of QDs. After gentle mixing, the sample was incubated at ∼4 °C for 1 h to allow self-assembly, and then diluted in DMEM culture media to a total volume of 500 μL. This refers to the final volume and concentration applied to the cell cultures. The conjugate formation was first confirmed in vitro using affinity chromatography, i.e., binding to amylose and release by added maltose. Here, a plastic column was first loaded with 1 mL of amylose gel. After settling the gel was rinsed with a 10 mL of PBS buffer (pH 7) to remove the residual ethanol contained in the commercial gel stock solution. When loaded the conjugates were immobilized on top of the amylose column and stayed bound even after several washes with buffer. The MBP promoted binding of the conjugates to the column due to its specific affinity to amylose, while the QDs allowed fluorescent visualization (colored green band) of the reagents in the column (see Figure 1B). Addition of 2−3 mL of 20 mM maltose solution readily displaced the reagents until complete elution. These two processes combined indicate that QD-MBP-γ conjugates are formed and that the MBP maintained its biological activity.

Cellular Uptake of Quantum Dot−MBP-Lytic Peptide Assemblies. 8×10^4 cells were seeded onto 12 mm circle microcover glasses placed into 24-well microtiter plates (CellStar, VWR), and the plates were placed in an incubator overnight to allow attachment and recovery. After 24 h, the QDs, QD-MBP, or QD-γ-MBP bioconjugates, diluted into culture medium (DMEM without Phenol Red, Invitrogen) to the desired concentrations, were added to the cell culture. Cultures were then incubated for different times (at 37 or 4 °C). Cy5-transferrin marker (at 40 μg/mL) was also added to the culture to specifically identify the late endosomal/lysosomal compartments. Excess unbound QD materials and Cy5 were removed by washing three times with phosphate-buffered saline (PBS, pH 7.4). The cells were then fixed in 3.7% paraformaldehyde for 12 min at room temperature, washed, and mounted in ProLong Antifade mounting media containing DAPI dye (Invitrogen) for nuclear staining, then imaged using epifluorescence and/or confocal microscopy.

Epifluorescence images of the fixed cells were collected using a Nikon Ti-E inverted microscope equipped with an Intensilight C-HGFI illuminator and a Photometrics Cool Snap HQ2 camera (Photometrics). Images were collected using a 40× objective (Nikon) and a set of filter cubes purchased from Chroma Technology (Rockingham, VT). Excitation of all samples was provided by a Xe lamp. DAPI fluorescence was detected using a DAPI cube (D350/50× for excitation, dichroic 400DCLP, and D460/50m for detection). The QD fluorescence signal (peak at 540 nm) was detected using a GFP/EGFP cube (HQ470/40× for excitation, dichroic Q495lp, and HQ525/50m for detection), while the Cy5 emission was detected using Cy5 cube (HQ560/55× for excitation, dichroic Q595lp, and HQ645/75 for detection). The images were analyzed and processed using NIS-Elements Advanced Research (Nikon) and Photoshop Adobe (software). Differential interference contrast (DIC) images were collected using a bright light source.

DOI: 10.1021/acs.bioconjchem.6b00609
Bioconjugate Chem. 2017, 28, 64−74

The laser-scanning confocal microscopy images shown in Figure 4 were collected using an Olympus FV1000 microscope equipped with an Olympus PlanApo 60× oil immersion objective (NA = 1.4), available at the National High Magnetic Laboratory (NHMFL), Tallahassee. Blue DAPI-type fluorescence was excited using a 405 nm diode laser and detected through a variable bandpass filter (VBF) with a detection slit setting of 430−490 nm. Green fluorescence from the quantum dots was excited using a 405 nm diode laser and detected with a slit setting of 550−610 nm. Far-red fluorescence from Cy5-transferrin was excited using a 633 nm helium−neon laser and detected using a 650 nm long-pass emission filter. Blue and green fluorescence were collected simultaneously (both excited by 405 nm laser) and sequentially with respect to the far-red fluorescence channel at a speed of 12.5 μs/pixel; the fluorescence was detected using a pinhole size of 110 μm. Image acquisition was performed using proprietary Olympus FluoView software.

Laser-scanning confocal microscopy images in Figure 6A were collected using a Leica TCS SP2 DM6000 microscope equipped with a Leica 63× oil immersion objective (NA = 1.4), available at the FSU School of Medicine. Blue DAPI and green fluorescence of the QDs were excited using a 405 nm diode laser and the emissions were detected using filter sets in the ranges 436−477 nm and 506−556 nm, respectively. The red fluorescence from Cy5-transferrin was excited using a 633 nm He−Ne laser, and the emission was detected in the range of 663−705 nm. The fluorescence emission was collected using an Acoustic Optical Tunable Filter (AOTF).

Flow Cytometry. Cells were treated with a 500 μL total volume of 50 nM of QD conjugates and nonconjugated QDs (control) for different incubation times. After trypsinization, cells were centrifuged at 1200 rpm for 5 min and resuspended in cell culture medium with 1 μg/mL propidium iodide 2 min before cytometric analysis. Forward scatter (FS), side scatters (SS), and propidium iodide (PI) fluorescence of individual cells incubated for various times with nanoparticles were measured on a BD FACSAria (SORP) flow cytometer. FS and SS intensities (measured at 488 nm) were digitized on linear and logarithmic scales (4 decades). Red fluorescence intensities emitted by dead cells (measured at 610 nm) was digitalized on a logarithmic scale. Cellular debris was eliminated by using a large gate in a FS versus SS cytogram. Dead cells and living cells were identified by their forward scatter and red fluorescence intensities. Samples were excited with an argon laser tuned to 405 nm line for fluorescence excitation, and emission was collected with a 525/50 bandpass emission filter.

■ ASSOCIATED CONTENT

Supporting Information

The Supporting Information is available free of charge on the ACS Publications website at DOI: 10.1021/acs.bioconjchem.6b00609.

Additional information and data on the peptide cloning, QD functionalization, conjugate self-assembly, affinity chromatography tests, absorption and fluorescence of the Cy5, cell culture, fluorescence imaging, viability assays, and conjugate uptake by 3T3 and HEK cells (PDF)

■ AUTHOR INFORMATION

Corresponding Author

*E-mail: mattoussi@chem.fsu.edu.

ORCID

Hedi Mattoussi: 0000-0002-6511-9323

Present Addresses

[#]Université Paris-Sud, Laboratoire de Physique des Solides, 1 rue Nicolas Appert, 91405 Orsay cedex, France

[¶]Virology Department, Federal University of Rio de Janeiro, Ilha Cidade Universitária - s/n bl I ss, Rio de Janeiro, 21941−970, Brazil

[■]Illumina Corp., 5200 Illumina Way, San Diego, CA 92122

[▽]Florida Department of Agriculture, Division of Food Safety, 3125 Conner Blvd. Lab 3, Tallahassee, FL 32399

Notes

The authors declare no competing financial interest.

■ ACKNOWLEDGMENTS

We thank FSU and the National Science Foundation (NSF-CHE, #1058957 and #1508501), NIH grant 5R01 GM 54076 to J.E.J., PEW Latin American Fellowship Program and Conselho Nacional de Desenvolvimento Cientifico (CNPq) Brasil (to T.D.) for financial support. The authors also acknowledge J. Allen for the confocal microscopy experiments performed at the High National Magnetic Field (FSU) and Ruth Didier for the flow cytometry analysis and the confocal microscopy experiments performed at the College of Medicine (FSU). We also thank G. Palui and X. Ji for the fruitful discussions.

■ REFERENCES

(1) Weissleder, R., Tung, C.-H., Mahmood, U., and Bogdanov, A. (1999) In vivo imaging of tumors with protease-activated near-infrared fluorescent probes. *Nat. Biotechnol. 17*, 375−378.

(2) McDonald, D., Vodicka, M. A., Lucero, G., Svitkina, T. M., Borisy, G. G., Emerman, M., and Hope, T. J. (2002) Visualization of the intracellular behavior of HIV in living cells. *J. Cell Biol. 159*, 441−452.

(3) Denk, W., Strickler, J., and Webb, W. (1990) Two-photon laser scanning fluorescence microscopy. *Science 248*, 73−76.

(4) Shaner, N. C., Steinbach, P. A., and Tsien, R. Y. (2005) A guide to choosing fluorescent proteins. *Nat. Methods 2*, 905−909.

(5) Miyawaki, A. (2011) Development of Probes for Cellular Functions Using Fluorescent Proteins and Fluorescence Resonance Energy Transfer. *Annu. Rev. Biochem. 80* (80), 357−373.

(6) Jun, Y. W., Lee, J. H., and Cheon, J. (2008) Chemical design of nanoparticle probes for high-performance magnetic resonance imaging. *Angew. Chem., Int. Ed. 47*, 5122−5135.

(7) Zrazhevskiy, P., Sena, M., and Gao, X. H. (2010) Designing multifunctional quantum dots for bioimaging, detection, and drug delivery. *Chem. Soc. Rev. 39*, 4326−4354.

(8) Mattoussi, H., Palui, G., and Na, H. B. (2012) Luminescent quantum dots as platforms for probing in vitro and in vivo biological processes. *Adv. Drug Delivery Rev. 64*, 138−166.

(9) Jaiswal, J. K., Mattoussi, H., Mauro, J. M., and Simon, S. M. (2002) Long-term multiple color imaging of live cells using quantum dot bioconjugates. *Nat. Biotechnol. 21*, 47−51.

(10) Dahan, M., Levi, S., Luccardini, C., Rostaing, P., Riveau, B., and Triller, A. (2003) Diffusion dynamics of glycine receptors revealed by single-quantum dot tracking. *Science 302*, 442−445.

(11) Michalet, X., Pinaud, F., Bentolila, L., Tsay, J., Doose, S., Li, J., Sundaresan, G., Wu, A., Gambhir, S., and Weiss, S. (2005) Quantum dots for live cells, in vivo imaging, and diagnostics. *Science 307*, 538−544.

(12) Medintz, I., Uyeda, H., Goldman, E., and Mattoussi, H. (2005) Quantum dot bioconjugates for imaging, labelling and sensing. *Nat. Mater. 4*, 435−446.

(13) Dabbousi, B. O., RodriguezViejo, J., Mikulec, F. V., Heine, J. R., Mattoussi, H., Ober, R., Jensen, K. F., and Bawendi, M. G. (1997)

DOI: 10.1021/acs.bioconjchem.6b00609
Bioconjugate Chem. 2017, 28, 64−74

CdSe)ZnS core-shell quantum dots: Synthesis and characterization of a size series of highly luminescent nanocrystallites. *J. Phys. Chem. B 101*, 9463−9475.
(14) Kovalenko, M. V., Bodnarchuk, M. I., Zaumseil, J., Lee, J. S., and Talapin, D. V. (2010) Expanding the Chemical Versatility of Colloidal Nanocrystals Capped with Molecular Metal Chalcogenide Ligands. *J. Am. Chem. Soc. 132*, 10085−10092.
(15) Wu, X. Y., Liu, H. J., Liu, J. Q., Haley, K. N., Treadway, J. A., Larson, J. P., Ge, N. F., Peale, F., and Bruchez, M. P. (2002) Immunofluorescent labeling of cancer marker Her2 and other cellular targets with semiconductor quantum dots. *Nat. Biotechnol. 21*, 41−46.
(16) Choi, H. S., Liu, W., Misra, P., Tanaka, E., Zimmer, J. P., Ipe, B. I., Bawendi, M. G., and Frangioni, J. V. (2007) Renal clearance of quantum dots. *Nat. Biotechnol. 25*, 1165−1170.
(17) Hattori, Y., and Maitani, Y. (2005) Folate-linked lipid-based nanoparticle for targeted gene delivery. *Curr. Drug Delivery 2*, 243−252.
(18) Muroski, M. E., Carnevale, K. J. F., Riskowski, R. A., and Strouse, G. F. (2015) Plasmid Transfection in Mammalian Cells Spatiotemporally Tracked by a Gold Nanoparticle. *ACS Nano 9*, 124.
(19) Torchilin, V. P. (2008) Tat peptide-mediated intracellular delivery of pharmaceutical nanocarriers. *Adv. Drug Delivery Rev. 60*, 548−558.
(20) Delehanty, J. B., Medintz, I. L., Pons, T., Brunel, F. M., Dawson, P. E., and Mattoussi, H. (2006) Self-Assembled Quantum Dot−Peptide Bioconjugates for Selective Intracellular Delivery. *Bioconjugate Chem. 17*, 920−927.
(21) Susumu, K., Uyeda, H. T., Medintz, I. L., Pons, T., Delehanty, J. B., and Mattoussi, H. (2007) Enhancing the stability and biological functionalities of quantum dots via compact multifunctional ligands. *J. Am. Chem. Soc. 129*, 13987−13996.
(22) Liu, B. R., Huang, Y. W., Winiarz, J. G., Chiang, H. J., and Lee, H. J. (2011) Intracellular delivery of quantum dots mediated by a histidine- and arginine-rich HR9 cell-penetrating peptide through the direct membrane translocation mechanism. *Biomaterials 32*, 3520−3537.
(23) Liu, B. R., Liou, J.-S., Huang, Y.-W., Aronstam, R. S., and Lee, H.-J. (2013) Intracellular Delivery of Nanoparticles and DNAs by IR9 Cell-penetrating Peptides. *PLoS One 8*, e64205.
(24) Falanga, A., Vitiello, M. T., Cantisani, M., Tarallo, R., Guarnieri, D., Mignogna, E., Netti, P., Pedone, C., Galdiero, M., and Galdiero, S. (2011) A peptide derived from herpes simplex virus type 1 glycoprotein H: membrane translocation and applications to the delivery of quantum dots. *Nanomedicine 7*, 925−934.
(25) Delehanty, J. B., Mattoussi, H., and Medintz, I. L. (2009) Delivering quantum dots into cells: strategies, progress and remaining issues. *Anal. Bioanal. Chem. 393*, 1091−1105.
(26) Derfus, A. M., Chan, W. C. W., and Bhatia, S. N. (2004) Intracellular delivery of quantum dots for live cell labeling and organelle tracking. *Adv. Mater. 16*, 961.
(27) Medintz, I. L., Pons, T., Delehanty, J. B., Susumu, K., Brunel, F. M., Dawson, P. E., and Mattoussi, H. (2008) Intracellular Delivery of Quantum Dot−Protein Cargos Mediated by Cell Penetrating Peptides. *Bioconjugate Chem. 19*, 1785−1795.
(28) Lee, J., Sharei, A., Sim, W. Y., Adamo, A., Langer, R., Jensen, K. F., and Bawendi, M. G. (2012) Nonendocytic Delivery of Functional Engineered Nanoparticles into the Cytoplasm of Live Cells Using a Novel, High-Throughput Microfluidic Device. *Nano Lett. 12*, 6322−6327.
(29) Agrawal, D. K., and Johnson, J. E. (1992) Sequence and Analysis of the Capsid Protein of Nudaurelia-Capensis Omega-Virus, an Insect Virus with T = 4 Icosahedral Symmetry. *Virology 190*, 806−814.
(30) Moyer, C. L., and Nemerow, G. R. (2011) Viral weapons of membrane destruction: variable modes of membrane penetration by non-enveloped viruses. *Curr. Opin. Virol. 1*, 44−49.
(31) Canady, M. A., Tihova, M., Hanzlik, T. N., Johnson, J. E., and Yeager, M. (2000) Large conformational changes in the maturation of a simple RNA virus, Nudaurelia capensis omega virus (N omega V). *J. Mol. Biol. 299*, 573−584.
(32) Domitrovic, T., Matsui, T., and Johnson, J. E. (2012) Dissecting quasi-equivalence in nonenveloped viruses: membrane disruption is promoted by lytic peptides released from subunit pentamers, not hexamers. *Journal of Virology 86*, 9976−9982.
(33) Medintz, I. L., Konnert, J. H., Clapp, A. R., Stanish, I., Twigg, M. E., Mattoussi, H., Mauro, J. M., and Deschamps, J. R. (2004) A fluorescence resonance energy transfer-derived structure of a quantum dot-protein bioconjugate nanoassembly. *Proc. Natl. Acad. Sci. U. S. A. 101*, 9612−9617.
(34) Zhan, N. Q., Palui, G., Safi, M., Ji, X., and Mattoussi, H. (2013) Multidentate Zwitterionic Ligands Provide Compact and Highly Biocompatible Quantum Dots. *J. Am. Chem. Soc. 135*, 13786−13795.
(35) Lowe, S. B., Dick, J. A. G., Cohen, B. E., and Stevens, M. M. (2012) Multiplex Sensing of Protease and Kinase Enzyme Activity via Orthogonal Coupling of Quantum Dot Peptide Conjugates. *ACS Nano 6*, 851−857.
(36) Ghadiali, J. E., Cohen, B. E., and Stevens, M. M. (2010) Protein Kinase-Actuated Resonance Energy Transfer in Quantum Dot-Peptide Conjugates. *ACS Nano 4*, 4915−4919.
(37) Zhan, N., Palui, G., Grise, H., Tang, H., Alabugin, I., and Mattoussi, H. (2013) Combining Ligand Design with Photoligation to Provide Compact, Colloidally Stable, and Easy to Conjugate Quantum Dots. *ACS Appl. Mater. Interfaces 5*, 2861−2869.
(38) Clapp, A. R., Goldman, E. R., and Mattoussi, H. (2006) Capping of CdSe-ZnS quantum dots with DHLA and subsequent conjugation with proteins. *Nat. Protoc. 1*, 1258−1266.
(39) Pons, T., Uyeda, H. T., Medintz, I. L., and Mattoussi, H. (2006) Hydrodynamic dimensions, electrophoretic mobility, and stability of hydrophilic quantum dots. *J. Phys. Chem. B 110*, 20308−20316.
(40) Delehanty, J. B., Bradburne, C. E., Boeneman, K., Susumu, K., Farrell, D., Mei, B. C., Blanco-Canosa, J. B., Dawson, G., et al. (2010) Delivering quantum dot-peptide bioconjugates to the cellular cytosol: escaping from the endolysosomal system. *Integrative Biology 2*, 265−277.
(41) Wang, W., Kapur, A., Ji, X., Zeng, B., Mishra, D., and Mattoussi, H. (2016) Multifunctional and High Affinity Polymer Ligand that Provides Bio-Orthogonal Coating of Quantum Dots. *Bioconjugate Chem. 27*, 2024−2036.
(42) Heuser, J. E., and Anderson, R. G. (1989) Hypertonic media inhibit receptor-mediated endocytosis by blocking clathrin-coated pit formation. *J. Cell Biol. 108*, 389−400.
(43) Park, R. D., Sullivan, P. C., and Storrie, B. (1988) Hypertonic sucrose inhibition of endocytic transport suggests multiple early endocytic compartments. *J. Cell. Physiol. 135*, 443−450.
(44) Schmid, S. L., and Carter, L. L. (1990) ATP is required for receptor-mediated endocytosis in intact cells. *J. Cell Biol. 111*, 2307−2318.
(45) Medina, S. H., and Schneider, J. P. (2015) Cancer cell surface induced peptide folding allows intracellular translocation of drug. *J. Controlled Release 209*, 317−326.
(46) Tan, R. S., Naruchi, K., Amano, M., Hinou, H., and Nishimura, S. (2015) Rapid Endolysosomal Escape and Controlled Intracellular Trafficking of Cell Surface Mimetic Quantum-Dots-Anchored Peptides and Glycopeptides. *ACS Chem. Biol. 10*, 2073−2086.
(47) Anas, A., Okuda, T., Kawashima, N., Nakayama, K., Itoh, T., Ishikawa, M., and Biju, V. (2009) Clathrin-mediated endocytosis of quantum dot-peptide conjugates in living cells. *ACS Nano 3*, 2419−2429.
(48) Wang, W., Kapur, A., Ji, X., Safi, M., Palui, G., Palomo, V., Dawson, P. E., and Mattoussi, H. (2015) Photoligation of an Amphiphilic Polymer with Mixed Coordination Provides Compact and Reactive Quantum Dots. *J. Am. Chem. Soc. 137*, 5438−5451.
(49) Lagerholm, B. C., Wang, M. M., Ernst, L. A., Ly, D. H., Liu, H. J., Bruchez, M. P., and Waggoner, A. S. (2004) Multicolor coding of cells with cationic peptide coated quantum dots. *Nano Lett. 4*, 2019−2022.
(50) Pelley, J. L., Daar, A. S., and Saner, M. A. (2009) State of Academic Knowledge on Toxicity and Biological Fate of Quantum Dots. *Toxicol. Sci. 112*, 276−296.

DOI: 10.1021/acs.bioconjchem.6b00609
Bioconjugate Chem. 2017, 28, 64−74

(51) Hauck, T. S., Anderson, R. E., Fischer, H. C., Newbigging, S., and Chan, W. C. W. (2010) In vivo Quantum-Dot Toxicity Assessment. *Small 6*, 138−144.
(52) Bharali, D. J., Lucey, D. W., Jayakumar, H., Pudavar, H. E., and Prasad, P. N. (2005) Folate-receptor-mediated delivery of InP quantum dots for bioimaging using confocal and two-photon microscopy. *J. Am. Chem. Soc. 127*, 11364−11371.
(53) Lidke, D. S., Nagy, P., Heintzmann, R., Arndt-Jovin, D. J., Post, J. N., Grecco, H. E., Jares-Erijman, E. A., and Jovin, T. M. (2004) Quantum dot ligands provide new insights into erbB/HER receptor-mediated signal transduction. *Nat. Biotechnol. 22*, 198−203.
(54) Chan, W. C. W., and Nie, S. M. (1998) Quantum dot bioconjugates for ultrasensitive nonisotopic detection. *Science 281*, 2016−2018.
(55) Zhang, Y., So, M. K., and Rao, J. H. (2006) Protease-modulated cellular uptake of quantum dots. *Nano Lett. 6*, 1988−1992.
(56) Chakraborty, S. K., Fitzpatrick, J. A. J., Phillippi, J. A., Andreko, S., Waggoner, A. S., Bruchez, M. P., and Ballou, B. (2007) Cholera toxin B conjugated quantum dots for live cell Labeling. *Nano Lett. 7*, 2618−2626.
(57) Munshi, S., Liljas, L., Cavarelli, J., Bomu, W., McKinney, B., Reddy, V., and Johnson, J. E. (1996) The 2.8 angstrom structure of a T = 4 animal virus and its implications for membrane translocation of RNA. *J. Mol. Biol. 261*, 1−10.
(58) Matsui, T., Tsuruta, H., and Johnson, J. E. (2010) Balanced Electrostatic and Structural Forces Guide the Large Conformational Change Associated with Maturation of T = 4 Virus. *Biophys. J. 98*, 1337−1343.
(59) Zhang, Y. J., Zheng, F., Yang, T. L., Zhou, W., Liu, Y., Man, N., Zhang, L., Jin, N., Dou, Q. Q., and Zhang, Y. (2012) Tuning the autophagy-inducing activity of lanthanide-based nanocrystals through specific surface-coating peptides. *Nat. Mater. 11*, 817−826.
(60) Tsai, T. L., Hou, C. C., Wang, H. C., Yang, Z. S., Yeh, C. S., Shieh, D. B., and Su, W. C. (2012) Nucleocytoplasmic transport blockage by SV40 peptide-modified gold nanoparticles induces cellular autophagy. *Int. J. Nanomed. 7*, 5215−5234.
(61) Wei, P. F., Zhang, L., Lu, Y., Man, N., and Wen, L. P. (2010) C60(Nd) nanoparticles enhance chemotherapeutic susceptibility of cancer cells by modulation of autophagy. *Nanotechnology 21*, 495101.
(62) Aldeek, F., Safi, M., Zhan, N., Palui, G., and Mattoussi, H. (2013) Understanding the Self-Assembly of Proteins onto Gold Nanoparticles and Quantum Dots Driven by Metal-Histidine Coordination. *ACS Nano 7*, 10197−10210.
(63) Mattoussi, H., Cumming, A. W., Murray, C. B., Bawendi, M. G., and Ober, R. (1998) Properties of CdSe nanocrystal dispersions in the dilute regime: Structure and interparticle interactions. *Phys. Rev. B: Condens. Matter Mater. Phys. 58*, 7850−7863.
(64) Yu, W. W., and Peng, X. G. (2002) Formation of high-quality CdS and other II-VI semiconductor nanocrystals in noncoordinating solvents: Tunable reactivity of monomers. *Angew. Chem., Int. Ed. 41*, 2368−2371.
(65) Reiss, P., Protiere, M., and Li, L. (2009) Core/Shell Semiconductor Nanocrystals. *Small 5*, 154−168.
(66) Palui, G., Avellini, T., Zhan, N., Pan, F., Gray, D., Alabugin, I., and Mattoussi, H. (2012) Photoinduced Phase Transfer of Luminescent Quantum Dots to Polar and Aqueous Media. *J. Am. Chem. Soc. 134*, 16370−16378.

DOI: 10.1021/acs.bioconjchem.6b00609
Bioconjugate Chem. 2017, 28, 64−74